Pergamon

Geochimica et Cosmochimica Acta, Vol. 67, No. 3, pp. 459–471, 2003

0016-7037/03 $22.00 + .00

PII S0016-7037(02)01090-6

Experimental determination of oxygen isotope fractionations between CO_2 vapor and soda-melilite melt

IRMA APPORA,[1,*,†] JOHN. M EILER,[1] ALAN MATTHEWS,[2] and EDWARD M. STOLPER[1]

[1]Division of Geological and Planetary Sciences, MC 170-25, California Institute of Technology, Pasadena, CA, 91125, USA
[2]Institute of Earth Sciences, Hebrew University of Jerusalem, 91904 Jerusalem, Israel

(*Received March* 1, 2002; *accepted in revised form July* 30, 2002)

Abstract—We report results of experiments constraining oxygen isotope fractionations between CO_2 vapor and Na-rich melilitic melt at 1 bar and 1250 and 1400°C. The fractionation factor constrained by bracketed experiments, $1000 \cdot \ln\alpha_{CO2\text{-}Na\ melilitic\ melt}$, is 2.65±0.25 ‰ (±2$\sigma$; n=92) at 1250°C and 2.16±0.16 ‰ (2σ; n=16) at 1400°C. These values are independent of Na content over the range investigated (7.5 to 13.0 wt. % Na_2O). We combine these data with the known reduced partition function ratio of CO_2 to obtain an equation describing the reduced partition function ratio of Na-rich melilite melt as a function of temperature. We also fit previously measured CO_2-melt or -glass fractionations to obtain temperature-dependent reduced partition function ratios for all experimentally studied melts and glasses (including silica, rhyolite, albite, anorthite, Na-rich melilite, and basalt). The systematics of these data suggest that reduced partition function ratios of silicate melts can be approximated either by using the Garlick index (a measure of the polymerization of the melt) or by describing melts as mixtures of normative minerals or equivalent melt compositions. These systematics suggest oxygen isotope fractionation between basalt and olivine at 1300°C of approximately 0.4 to 0.5‰, consistent with most (but not all) basalt glass-olivine fractionations measured in terrestrial and lunar basalts.

1. INTRODUCTION

Oxygen isotope ratios of igneous rocks constrain the relative proportions of crustal and mantle materials in their sources (e.g., Taylor and Sheppard, 1986; Eiler, 2001). However, these ratios are also influenced by isotopic fractionations during partial melting, crystallization-differentiation, and degassing. These fractionations must be quantified before oxygen isotope variations can be used as fingerprints for the sources of igneous rocks. Oxygen isotope fractionations among silicate melts, their phenocrysts and exsolved gases, and residual minerals in their source region are small at magmatic temperatures (typically ≤ 1 to 2 ‰ for major phases). Consequently, they can generally be neglected when variations in $\delta^{18}O$ are large, as in suites of crustally contaminated igneous rocks (e.g., Davidson and Harmon 1989). However, these magmatic fractionations are similar in magnitude to the range in $\delta^{18}O$ exhibited by basalts, their phenocrysts, and mantle rocks (Eiler, 2001). Thus, detailed interpretations of oxygen isotope variations of these materials require measurements of oxygen isotope fractionations involving silicate liquids.

There are many previous studies of oxygen isotope fractionations in mineral-mineral and fluid-mineral systems (e.g., Bottinga and Javoy, 1975; Deines, 1977; Matthews et al., 1983; Clayton et al., 1989; Chiba et al., 1989; see Chacko et al., 2001 for review) and these studies are in good agreement for many of the rock-forming minerals. In contrast, oxygen isotope fractionations involving silicate melts or glasses are less well known and generally have been dealt with by assuming that they can be approximated by fractionations involving chemically similar minerals (e.g., Matsuhisa et al., 1979; Kalamarides, 1986). Experiments on felsic melts and glasses have validated this approximation in some cases (Palin et al., 1996; Matthews et al., 1994, 1998) but not others (Stolper and Epstein, 1991). Fractionations involving basic and ultrabasic melts are particularly poorly known, having been measured in only one experimental study (Muehlenbachs and Kushiro, 1974).

We report here measurements of oxygen isotopic fractionations between CO_2 vapor and Na-rich melilitic melts at 1 bar, 1250 to 1400°C. We chose these melt compositions because they are structural analogues for tholeiitic basalt (Mysen, 1980; Kohn, 1991) and are predicted to have oxygen isotope partitioning behaviors broadly similar to that of basalt (Matthews et al., 1998). Such melts have the advantage, however, of not undergoing the Fe-loss that can complicate experiments on basaltic melts. In addition to reporting our results, we compare them to those of previous studies of oxygen isotope fractionations involving silicate glasses and melts, derive a set of internally consistent equations describing reduced partition function ratios of these glasses and melts as functions of temperature, and discuss methods for interpolating these data to estimate reduced partition function ratios of other silicate melt compositions.

2. MATERIAL AND METHODS

2.1. Starting Materials

All experiments reported here were conducted on one of six compositionally and/or isotopically distinct Na-rich melilitic glasses. Major-element and oxygen isotope compositions of glass starting materials used in this study are reported in Table 1. NaMel/1 is a glass prepared to our specifications by the Corning laboratories by fusion of oxide and

* Author to whom correspondence should be addressed (appora@ipgp.jussieu.fr).
† *Present address:* Laboratoire de Géochimie des Isotopes Stables, Université de Paris 7 Denis Diderot, IPGP CNRS 1762, 2 place Jussieu, 75251, Paris Cedex 05, France.

Table 1. Starting glasses, Major-element and oxygen isotope compositions

Starting Glass	$\delta^{18}O$ ‰ (2σ)	SiO_2‡ wt.% (2σ)	Al_2O_3‡ wt.% (2σ)	CaO‡ wt.% (2σ)	Na_2O‡ wt.% (2σ)
NaMel/1	11.96 (0.30)	46.98 (0.92)	20.12 (0.78)	20.91 (0.92)	11.88 (0.78)
NaMel/2	−6.32 (0.33)	47.84 (1.82)	20.78 (0.53)	21.48 (0.85)	9.78 (0.39)
NaMel/3	−3.63 (0.20)	47.63 (0.78)	20.80 (0.60)	21.83 (0.62)	9.61 (0.90)
NaMel/4	9.17 (0.18)	43.44 (0.54)	19.86 (0.14)	19.52 (0.13)	17.04 (0.46)
NaMel/6	9.72 (0.24)	40.73 (1.00)	18.82 (0.29)	18.27 (0.40)	22.07 (1.60)
NaMel/7	−6.11 (0.56)	47.30 (0.77)	20.49 (0.34)	21.49 (0.38)	10.59 (0.10)

All glasses contain ~0.1 wt. % MgO
‡ average of analyses on multiple glasses (see details on analytical paragraph) normalized to a 100 wt.% total oxides

carbonate powders in a Pt crucible. Its major-element composition, as determined by electron microprobe, closely approaches the intended stoichiometry: $NaCaAlSi_2O_7$ (the actual stoichiometry is $Na_{0.98}Ca_{0.95}AlSi_2O_7$). The $\delta^{18}O$ value of NaMel/1, as determined by laser fluorination, is 11.96 ±0.30 ‰ (2σ, n = 47). Small quantities of the other five starting materials were prepared by various pretreatments of NaMel/1: NaMel/2, NaMel/3, and NaMel/7 were produced by exposing NaMel/1 to CO_2 of known and distinct $\delta^{18}O$ values for 24 to 28 h at 1250±5°C in a Deltech® DT-31 furnace. NaMel/4 and NaMel/6 were prepared by mixing dried Na_2CO_3 powder with powdered NaMel/1 in various proportions. These mixtures were then finely ground, re-dried, decarbonated by gradually heating from 150 to 600°C, and finally melted at 1280°C, homogenized at 1450°C for 8 h, and quenched by dropping into water. After preparation, each starting material was crushed in a stainless steel mortar and sieved to isolate a 0.5 to 1 mm size fraction. Gaseous CO_2 used in these experiments was taken from high-pressure tanks obtained from Air Liquide Corporation and having a nominal purity of 99.8%.

2.2. Experimental Protocols

The following description of our experimental protocols refers to the apparatus illustrated in Figure 1. Single fragments of glass weighing 0.9 to 2.4 mg were hand picked from the 0.5 to 1 mm size fractions of the starting materials and loosely wrapped in 0.1 mm diameter Pt wire (99.998% nominal purity). These Pt-wound shards were suspended in a vertical Deltech® DT-31 furnace held at 1250 or 1400°C (all starting materials were molten at both temperatures) while continuously purging the furnace with a stream of CO_2 gas from a high-pressure tank, regulated to a small positive pressure. Flow rates of CO_2 gas into the furnace were set at 160, 190, or 500 cc/min. These flow rates correspond to gas velocities in the furnace of 0.32, 0.39 and 1.00 cm/s, respectively—all within the range required to prevent thermal convection of gas within the furnace (Darken, 1945; Huebner, 1975). The molar oxygen ratio between gas and melt (i.e., moles of oxygen in all CO_2 passed through the furnace over the course of an experiment divided by moles of oxygen from all glasses suspended in the furnace)

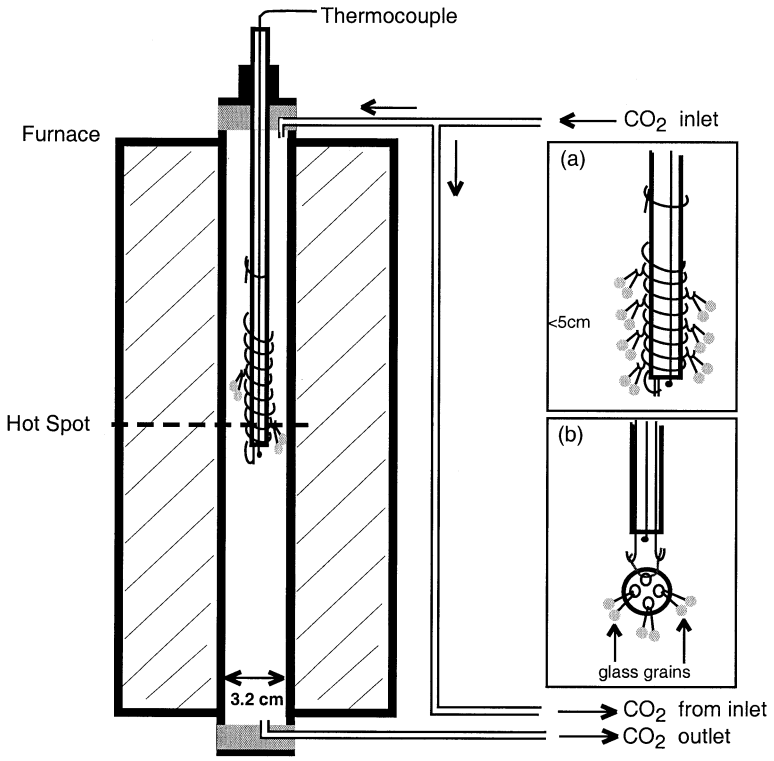

Fig. 1. Schematic illustration of the apparatus used for experiments described in this paper. A vertical section through center of the furnace shows the gas circulation and the positions of samples during an experiment. The furnace core and heating elements are within the dashed lines. Insets (a) and (b) show two different configurations for introducing glass samples to the furnace; see text for discussion.

was in the range of 10^3 to 10^5. Temperatures in the hot zone of the furnace adjacent to the glass samples were measured using a Pt-$Pt_{90}Rh_{10}$ (type S) thermocouple calibrated against the melting point of gold; we estimate the accuracy of these measurements to be ± 3°C. The temperature gradient within the furnace over the distance of the samples (typically ~5 cm) was 5°C (from the maximum temperature in the hot zone to lower temperatures above and below) at 1250°C and 10°C at 1400°C. Experiments lasted 4 to 48 h at 1250°C and 7 to 8 h at 1400°C.

During each experiment, CO_2 gas was collected both before and after the furnace at the ports indicated in Figure 1. At the end of each experiment, the sample was quenched by one of several methods: removal from the furnace into air; drop-quenching into water; or drop-quenching into liquid nitrogen. Reasons for and differences among these quench methods are discussed below. Wire-wrapped glass samples were suspended in the furnace by one of two methods, depending on the means by which they were to be quenched (see inset to Fig. 1: (a) If the sample was to be quenched by removal from the furnace into air, numerous (up to 40) samples were hung on hooks that were attached to a Pt spiral wound around an alumina tube and the entire assembly inserted into the furnace. Samples of the same starting material were often suspended together on the same hook so that they could be combined for a single isotope ratio analysis without concern that they experienced significantly different temperatures during the experiment. (b) If the sample was to be drop-quenched into water or liquid nitrogen, the wire-wrapped glass samples were hung on an alumina washer that was itself suspended by a length of Pt wire that could be melted by passing an electric current through it. We could only conduct experiments on a small number (typically 9) samples simultaneously using this protocol, but it provides a check on potential artifacts of air-quenched experiments.

Several combinations of CO_2 gas and glassy starting materials were used in our experiments at any given temperature, such that isotopic exchange between gas and melt proceeded from both directions (i.e., in some cases the $\delta^{18}O$ of the CO_2 was in initially higher than that of the starting glass and in other cases it was lower). When experiments that differ from one another in these ways yield indistinguishable final fractionations between the two phases undergoing isotopic exchange (i.e., gas and melt in this case), the observed fractionation is referred to as 'bracketed' or 'reversed' (O'Neil, 1986). Furthermore, the absolute value of the difference in $\delta^{18}O$ between the CO_2 gas and the glass starting material varied by ~20 per mil.

2.3. Analytical Techniques

The CO_2 vapor collected during experiments was cryogenically purified on a vacuum apparatus and analyzed for its isotopic composition on a Finnigan Mat 251 gas-source isotope-ratio mass spectrometer. Values of $\delta^{18}O$ are reported in units of per mil relative to SMOW (Baertschi, 1976). Values of $\delta^{18}O$ for pure CO_2 gases analyzed on this instrument have analytical uncertainties of 0.06 ‰ (2σ) based on long-term external reproducibility of in-house reference gases. The isotopic composition of CO_2 gas varied within narrow limits (typically less than ± 0.1 ‰, 2σ) over the course of each experiment and was indistinguishable whether collected before or after the furnace, indicating that the CO_2 gas did not undergo significant isotopic fractionation or exchange with the Al_2O_3 furnace tube. The average oxygen isotope composition of CO_2 for each experiment is provided in Table 2; the individual measurements on which these averages are based (generally 4 to 16 samples, depending on the duration of the experiment) are available from the authors by request. A large subset of experiments was conducted over a period of several weeks during which the gas came from a single tank of CO_2 and did not vary in isotopic composition within the precision of our analyses (Table 2); we have assumed a single constant $\delta^{18}O$ value for the gas for this set of experiments.

Glasses recovered from quenched melts at the end of each experiment were separated from the Pt wires (although generally some Pt remained) and combined with other glasses quenched from the same starting materials in quantities suitable for oxygen isotope analysis (~1 mg); this generally required combining two adjacent fragments of glass. Our minimum sample size for these measurements was dictated by the amount of glass required to overcome the analytical blank associated with laser fluorination of Na-rich glass. These glasses were analyzed for their oxygen isotope composition by laser fluorination at Caltech using a 50-W CO_2 laser, BrF_5 as the reagent and a Pt-graphite reactor to convert O_2 into CO_2. The data were standardized using silicate standards (SCO and UW Garnet; see Eiler et al., 1995 and Valley et al., 1995); measurements made on separate days were normalized to a common value of 5.25 ‰ for the San Carlos Olivine (SCO) standard. After normalization, reproducibility for SCO over the period of analysis was ± 0.15 (2σ, n = 106). Values of $\delta^{18}O$ for starting materials are reported in Table 1; values for glasses recovered at the end of experiments in Table 2. Values of $\delta^{18}O$ for glasses of the same starting material that were exposed to CO_2 in the furnace at the same time are averaged together in Table 2; the number of separate analyses contributing to each average is also indicated. However, we considered each determination to be a separate experiment for the purposes of reporting numbers of independent experiments and for calculating averages, standard deviations, and standard errors of CO_2-melt fractionations.

Major element (Si, Al, Ca, Na and K) abundances in starting materials and recovered glasses not selected for isotope ratio measurements were analyzed with a JEOL733 Superprobe using a 15 keV accelerating voltage, a 10 nÅ beam current, and a 20 μm spot. X-ray counts were collected for 30 s on peak and 15 s at each background position (a total of 120 s per analysis). Data were reduced using a CITZAF correction procedure (Armstrong 1995). Crystalline albite, anorthite, and forsterite were used as standards. We evaluated Na loss from the glasses during analysis by consecutive analyses of the same spot. For the settings given above, no significant decrease Na counts was observed over the first 250 s of analysis, suggesting that the Na_2O contents we report for shorter analyses are accurate. We performed multiple (typically 3 to 10) analyses for each grain. Based on numerous analyses on two samples over the period of the study, we estimate the precision of these measurements to be 0.9% for SiO_2, 1.5% for Al_2O_3, 2.4% for Ca_2O, 2.6% for Na_2O (all uncertainties are the 2σ error normalized to the amount present). Concentrations of K_2O are $<0.15 \pm 0.05$ (2σ) wt. %. Average major-element compositions of all starting materials are reported in Table 1. Na_2O contents of run products are reported in Table 2. Abundances of other major elements simply increase and decrease according to Na variations (for details on sodium behavior, see below); however, (Al_2O_3/SiO_2) and (CaO/SiO_2) ratios of both starting materials and run products are similar and range respectively from 0.41 to 0.46 and from 0.42 to 0.47. Na_2O concentrations are independent of the distance from the grain rim and approximately homogeneous within analytical uncertainties. Full major-element analyses of each run product are available on request from the authors. Note that Na_2O contents of experimental products reported in Table 2 are for glass fragments that hung adjacent to those analyzed for $\delta^{18}O$ during a given experiment. This introduces a level of ambiguity to the comparison of $\delta^{18}O$ and major element chemistry in the run products, but for reasons discussed below, this does not influence our conclusions.

3. RESULTS

Experimental results, including oxygen isotope composition of CO_2 gas averaged over several measurements made over the course of each experiment and average Na_2O contents and oxygen isotope compositions of quenched glass run products, are presented in Table 2. Complete chemical and isotopic analyses of each sample contributing to these averages are available on request from the authors. Also reported in Table 2 are fractionations $\Delta^{18}O_{CO2\text{-}melt}$ calculated as $= 1000 \cdot \ln\alpha_{CO2\text{-}melt}$. Statistical summaries of the results of all experiments are given in Table 3.

Most of our experiments were terminated by removing molten Na-rich melts from the furnace and allowing them to quench to glass in air. Experiments quenched in air were performed on glasses initially having between 9 and 12wt.% of Na_2O and using CO_2 flow rates of 160 or 190 cc/min. Sodium contents of glasses recovered at the end of experiments span a lower and more limited range in Na_2O contents (7.2 to 11.0 for

Table 2. Experimental conditions and results of experiments

Temperature	Exp.[§]	Duration	CO_2 gas Flow rate cc/min (±6%)	$\delta^{18}O_{SMOW}$ [measured][†] ‰ (2σ)	Na-melilite glass recovered: Initial batch	Na-melilite glass recovered: Na_2O[‡] wt.% (2σ)	Isotopic analysis no.[§]	$\delta^{18}O_{SMOW}$ ‰ (2σ)	Fractionation 1000 ln $\alpha_{(CO2\text{-}melt)}$ ‰ (2σ)	Quenching technique
1250°C										
	IA/22	4h	160	−1.00	NaMel/1			0.23	−1.23	cool in air
								−0.52	−0.48	
								−0.31	−0.69	
								0.97	−1.97	
					(*average*)	11.35 (0.73)				
					NaMel/2			−4.14	3.15	cool in air
								−4.65	3.66	
								−4.44	3.45	
								−4.13	3.13	
					(*average*)	10.02 (0.25)	4	−4.34 (0.51)		
					NaMel/3	–	4	−3.53 (0.06)	2.53 (0.16)	cool in air
	IA/24	16h	160	−1.00 [−0.96 ± 0.06]	NaMel/1	10.14 (0.56)	3	−3.65 (0.27)	2.66 (0.28)	cool in air
	IA/9[◇]	24h	160	−3.80 [±0.04]	NaMel/1	9.85 (0.25)	3	−6.33 (0.36)	2.55 (0.37)	cool in air
	IA/10[◇]	24h	160	−3.73 [±0.11]	NaMel/1	9.62 (0.25)	3	−6.30 (0.38)	2.58 (0.40)	cool in air
	IA/23	24h	160	−1.00 [−0.99 ± 0.03]	NaMel/1	10.30 (0.84)	2	−3.59 (0.46)	2.60 (0.46)	cool in air
					NaMel/2	9.72 (0.11)	3	−3.64 (0.08)	2.64 (0.16)	
					NaMel/3	9.63 (0.13)	4	−3.65 (0.22)	2.66 (0.23)	
	IA/14[◇]	28h	190	−1.00 [−1.01 ± 0.05]	NaMel/1	9.56 (0.78)	1	−3.56	2.56 (0.16)	cool in air
	IA/15[◇]	28h	190	−1.00 [−1.04 ± 0.05]	NaMel/1	–	1	−3.50	2.50 (0.16)	cool in air
	IA/16	28h	190	−1.00 [−1.01 ± 0.07]	NaMel/1	–	5	−3.66 (0.27)	2.67 (0.28)	cool in air
					NaMel/2	8.64 (0.08)	5	−3.58 (0.19)	2.58 (0.20)	
					NaMel/3	8.94 (0.15)	3	−3.55 (0.03)	2.56 (0.17)	
1250°C										
	IA/17[◇]	28h	190	−1.00 [−0.98 ± 0.05]	NaMel/1	10.17 (0.06)	3	−3.67 (0.24)	2.68 (0.24)	cool in air
	IA/18[◇]	28h	190	−1.00 [−1.02 ± 0.07]	NaMel/1	9.59 (1.24)	3	−3.66 (0.15)	2.67 (0.16)	cool in air
	IA/19	28h	160	−1.00 [−1.04 ± 0.07]	NaMel/1	9.59 (0.98)	5	−3.64 (0.12)	2.64 (0.17)	cool in air
					NaMel/2	9.40 (0.16)	3	−3.64 (0.06)	2.64 (0.17)	
					NaMel/3	9.80 (0.14)	4	−3.69 (0.10)	2.69 (0.17)	
	IA/26[∞]	32h	160	−1.00 [−1.00 ± 0.12]	NaMel/1	–	2	−3.44 (0.06)	2.45 (0.19)	cool in air
					NaMel/2	–	1	−3.35	2.36 (0.19)	
					NaMel/3	7.48 (0.24)		–		
	IA/20	38h	160	−1.00 [−0.99 ± 0.20]	NaMel/1	10.18 (0.35)	5	−3.71 (0.15)	2.72 (0.25)	cool in air
					NaMel/2	–	2	−3.88 (0.03)	2.89 (0.25)	
					NaMel/3	9.21 (0.96)	4	−3.77 (0.34)	2.77 (0.39)	
	IA/21	48h	160	−1.00 [−0.97 ± 0.11]	NaMel/1	10.13 (0.13)	5	−3.71 (0.38)	2.71 (0.39)	cool in air
					NaMel/2	9.74 (0.44)	4	−3.74 (0.25)	2.74 (0.27)	
					NaMel/3	9.24 (0.07)	3	−3.71 (0.19)	2.71 (0.22)	
	IA/35	28h	160	4.55 [4.54 ± 0.08]	NaMel/1	11.21 (0.12)	1	1.78	2.76 (0.17)	drop into H_2O
					NaMel/6	11.49 (0.20)	1	1.87	2.68 (0.17)	
					NaMel/7	11.33 (0.29)	1	1.88	2.66 (0.17)	
	IA/34	28h	500	4.55 [4.56 ± 0.01]	NaMel/1	–	1	1.96	2.58 (0.16)	drop into H_2O
					NaMel/6	11.21 (0.20)	1	1.80	2.74 (0.16)	
					NaMel/7	11.14 (0.12)	1	1.81	2.74 (0.16)	
	IA/42	28h	500	−2.46 [−2.46 ± 0.04]	NaMel/6	11.60 (0.31)	3	−5.09 (0.09)	2.64 (0.16)	drop into H_2O

(continued)

Table 2. (Continued)

Temperature	Exp.[§]	Duration	CO_2 gas Flow rate cc/min (±6%)	$\delta^{18}O_{SMOW}$ [measured][†] ‰ (2σ)	Na-melilite glass recovered: Initial batch	Na-melilite glass recovered: Na_2O[‡] wt.% (2σ)	Isotopic analysis no.[§]	Fractionation: $\delta^{18}O_{SMOW}$ ‰ (2σ)	Fractionation: 1000 ln $\alpha_{(CO2\text{-}melt)}$ ‰ (2σ)	Quenching technique
1250°C										
	IA/43	28h	500	−2.46 [−2.46 ± 0.04]	NaMel/4	11.15 (0.66)	3	−5.07 (0.23)	2.62 (0.24)	drop into H_2O
	IA/39	28h	500	1.56 [±0.06]	NaMel/1	10.09 (0.19)	1	−1.11	2.67 (0.16)	drop into N_2 liquid
					NaMel/6	10.70 (0.20)	1	−0.96	2.52 (0.16)	(but long quench)
					NaMel/7	9.94 (0.04)	1	−1.01	2.57 (0.16)	
	IA/40	28h	500	4.62 [4.61 ± 0.03]	NaMel/1	9.72 (0.20)	1	1.79	2.82 (0.16)	drop into N_2 liquid
					NaMel/6	11.12 (0.32)	1	1.82	2.79 (0.16)	
					NaMel/7	10.55 (0.15)	1	1.84	2.77 (0.16)	
1400°C										
	IA/25	7h	160	−1.00 [−0.93]	NaMel/1	8.43 (0.16)	3	−3.18 (0.20)	2.18 (0.21)	cool in air
					NaMel/2	8.40 (0.30)	3	−3.20 (0.25)	2.21 (0.26)	
					NaMel/3	8.62 (0.24)	3	−3.17 (0.18)	2.18 (0.19)	
	IA/36	8h	160	4.55 [4.56 ± 0.03]	NaMel/1	8.98 (0.23)	1	2.49	2.05 (0.16)	drop into H_2O
					NaMel/6	–	1	2.43	2.12 (0.16)	
	IA/37	8h	500	4.55 [4.56 ± 0.09]	NaMel/1	7.68 (0.14)	1	2.47	2.07 (0.17)	drop into H_2O
					NaMel/6	8.60 (0.07)	1	2.47	2.07 (0.17)	
					NaMel/7	8.39 (0.09)	1	2.35	2.19 (0.17)	
	IA/41	8h	500	4.62 [4.62 ± 0.06]	NaMel/1	7.57 (0.14)	1	–	–	Pull into air
					NaMel/6	7.72 (0.09)	1	2.37	2.24 (0.16)	then quenched
					NaMel/7	8.42 (0.15)	1	2.38	2.23 (0.16)	into N_2 liquid

Note.

[§] (abbreviations): Exp. = experiment; no. = number of analyses;

[†] isotopic composition of the CO_2 tank is the average of values measured during a time period of 3 to 4 days enclosing the experiment; numbers in brackets represent the isotopic composition of gas samples collected during the experiment itself;

[‡] average of analyses one or multiple glasses (see details on analytical paragraph) normalized to a 100 wt.% total oxides

[◇] run products from these experiments have been used as starting materials (as NaMel/2 or NaMel/3; see Table 1)

[∞] loading charge for experiments IA/26 consisted on 1/3 Na-melilite glasses. 1/3 CAS glasses and 1/3 diopside glass

Table 3. Oxygen equilibrium isotope fractionation between CO_2-gas and Na-rich melilite melt, based on the average of experimental results (statistical summary of results presented in Table 2)

	Run duration	Type of samples (no.)	Fractionation 1000 ln α(CO_2-melt) ‰ (2σ)
1250°C			
Air quenching experiments	≥ 24h	all analyses (no. = 74)	2.65 (0.26)
		reversal experiments (no. = 68)	2.67 (0.26)
		starting NaMel/1 (no. = 32)	2.65 (0.25)
		starting NaMel/2 (no. = 18)	2.66 (0.27)
		starting NaMel/3 (no. = 18)	2.68 (0.23)
	≥ 28h	all analyses (no. = 59)	2.67 (0.26)
		reversal experiments (no. = 51)	2.67 (0.27)
		starting NaMel/1 (no. = 30)	2.66 (0.25)
		starting NaMel/2 (no. = 15)	2.66 (0.30)
		starting NaMel/3 (no. = 14)	2.69 (0.23)
H_2O/N_2 quenching experiments	28h	all analyses (no. = 18)	2.67 (0.18)
		reversal experiments (no. = 12)	2.69 (0.18)
		H_2O drop quenching (no. = 12)	2.66 (0.15)
		N_2 liquid drop quenching (no. = 6)	2.69 (0.25)
		Ideal N_2 liquid drop quenching	see Exp. IA/40; Table 2
All experiments	≥ 24h	all analyses (no. = 92)	2.66 (0.25)
1400°C			
Air quenching experiments	7h	all analyses (no. = 9)	2.18 (0.20)
H_2O/N_2 quenching experiments	8h	all analyses of reversal experiments (no. = 7)	2.14 (0.16)
		H_2O drop quenching (no. = 5)	2.10 (0.11)
		N_2 liquid drop quenching	see Exp. IA/41; Table 2
All experiments	≥ 7h	all analyses (no. = 16)	2.17 (0.17)

Note. Abbreviations : Exp. = experiment; no. = number of analyses

experiments conducted at 1250°C and 8.2 to 8.8 wt. % for experiments conducted at 1400°C). The significance of sodium loss is discussed in a following section. Figures 2a and 2b plot measured $\Delta^{18}O_{CO2\text{-melt}}$ values versus the heating duration for all experiments conducted at 1250°C and quenched in air. Note that initial values of $\Delta^{18}O_{CO2\text{-melt}}$ define four groups with average values of −15.8, −13.0, 2.5 and 5.3 ‰, these values converge with a time constant of several hours, and within 24 h they define a common and time-invariant value of 2.65±0.26 ‰, (2σ, n=74). These data define a successfully 'bracketed' fractionation and therefore suggest that the average value of $\Delta^{18}O_{CO2\text{-melt}}$ observed after 24 h is the equilibrium value. We also conducted one set of air-quenched experiments at 1400°C lasting 7 h and including a range of starting glasses such that the results define a bracketed fractionation. The recovered glasses converged to a common $\delta^{18}O$ value defining a CO_2-melt fractionation of 2.18±0.20 ‰ (±2σ, n=9); we interpret this value as an equilibrium fractionation.

3.1. Evaluation of Quenching Artifacts

The major advantage of the air-quenching protocol we developed is that it allows simultaneous experiments on dozens of melt drops. It is, however, possible that this method could introduce a bias into our results because of oxygen isotope exchange between melt and air during the few seconds before temperature decreases sufficiently to form glass. We estimate based on simple models of diffusional exchange between air and melt that under extreme circumstances this process could lead to changes of up to several tenths of one per mil in the isotopic composition of quenched glass. Therefore, we also conducted experiments in which melt droplets were quenched in water or liquid nitrogen instead of air to determine whether there is a measurable dependence of our results on the method of quenching.

Drop-quench experiments were first held at high temperature in the furnace for sufficiently long times that we could be confident they reached gas-melt equilibrium before quenching (i.e., ≥24 h at 1250°C and ≥7 h at 1400°C). Drop-quench experiments were also distinguished from air-quenched experiments by generally higher CO_2 flow rates (500cc/min, except for one experiment conducted with CO_2 flow rate of 190cc/min) and by a greater range in initial Na_2O contents of from 10 to 22 wt.%. Despite these variations, recovered glasses exhibits a relatively small range in Na_2O content (i.e., 9.5 to 12.0 and 7.5 to 9.0 wt. % for experiments performed at 1200 and 1400°C, respectively) that is similar to that of air-quenched experiments. Processes of Na volatilization and their significance on isotopic results are evaluated in the following section. Isotopic results of these experiments are reported in Table 2, summarized along with air-quenched experiments in Table 3, and compared to air-quenched experiments in Figures 2c (1250°C experiments) and 2d (1400°C experiments). Experiments quenched in both water and liquid nitrogen define well-bracketed CO_2-melt fractionations, are indistinguishable from each other, and have average values of $\Delta^{18}O_{CO2\text{-melt}}$ of 2.67±0.18 ‰ (2σ, n=18) at 1250°C and 2.14±0.16 ‰ (2σ, n=8) at 1400°C. These results are indistinguishable from those for air-quenched experiments. Therefore, we conclude that our results are independent of the method of quenching and thus that quenching in air has had minimal effect on the $\delta^{18}O$ of the glass run products.

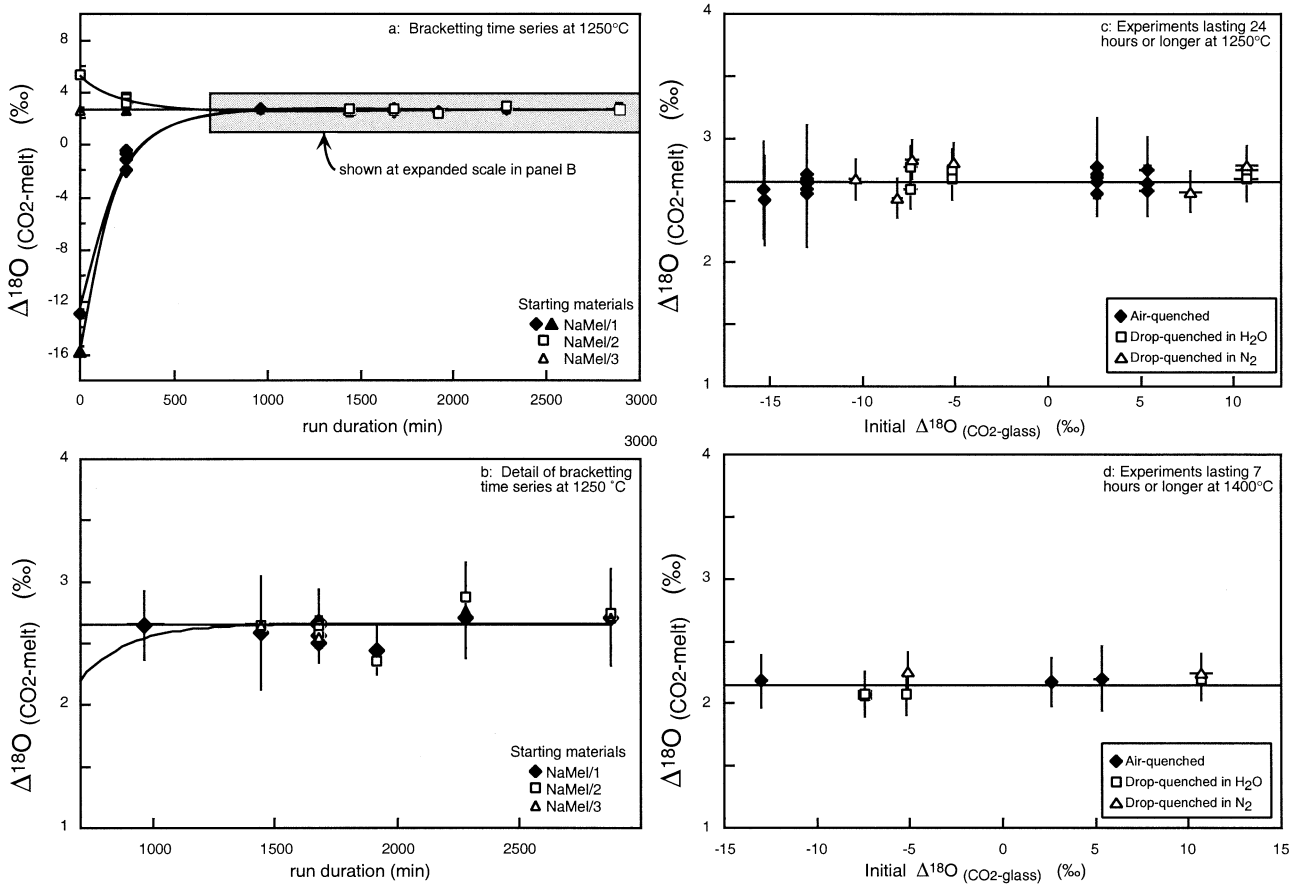

Fig. 2. (a) Variation with time of the oxygen isotope fractionation between CO_2 gas and Na-melilite melt during experiments for air-quenched experiments conducted at 1250°C. Filled diamonds and filled triangles are results for starting material NaMel/1; open squares are results for starting material NaMel/2; open triangles are data for starting material NaMel/3. Solid curves connect sets of experiments having similar initial differences in $\delta^{18}O$ between CO_2 gas and loaded glass. All data points are averages of multiple measured CO_2-melt fractionations for experiments using the same starting materials and conducted at the same time (see Table 2). The gray field surrounded by a dashed box shows the portion of this figure expanded in panel b. (b) Expanded view of data for experiments lasting longer than approximately 10 h. Errors bars are $\pm 2\sigma$. (c) Measured fractionations between CO_2 and Na-melilite melt for air- and drop-quenched experiments conducted at 1250°C and lasting 24 h or longer, plotted vs. the initial difference in $\delta^{18}O$ between CO_2 and starting glass. Error bars are $\pm 2\sigma$. Filled diamonds are air-quenched experiments (reproduced from Figs. 2a and 2b), unfilled squares are experiments drop-quenched into water; unfilled triangles are experiments drop-quenched into liquid nitrogen. (d) Measured fractionations between CO_2 and Na-melilite melt for air- and drop-quenched experiments conducted at 1400°C and lasting 7 h or longer, plotted vs. the initial difference in $\delta^{18}O$ between CO_2 and starting glass. Error bars and symbols are as in panel c.

3.2. Relationship of $\Delta^{18}O_{CO_2}$-melt to Na Abundance in and Loss from Melt

The extent of sodium loss from Na-melilite glasses over the course of our experiments varies with grain size, temperature and initial sodium content of those glasses; these dependencies are expected based on previous studies on Na volatilization from silicate melts (e.g., Donaldson, 1975; Corrigan and Gibb, 1979; Donaldson, 1979; Tsuchiyama et al., 1981). In particular: we find that if all other variables are held constant, the smallest glass grains (0.9 mg) lose ca. 1 wt. % more Na_2O than the largest (2.4 mg); experiments conducted at 1400°C consistently resulted in ca. 1.5 to 2 times greater sodium loss than did experiments conducted at 1250°C; and the wt. % Na_2O lost from the most sodium-rich starting glasses was up to several times greater than that from the least sodium-rich starting glasses. Finally, glasses with initially different sodium contents approach a common major-element composition (in some cases including increases of Na-poor glasses loaded adjacent to Na-rich glasses) over the course of an experiment, suggesting that Na is not only lost but also exchanged between adjacent melt drops.

Variations in Na contents of run-product glasses might influence their measured $\delta^{18}O$ values for two reasons: (1) variations in Na content of silicate melts might influence their reduced partition function ratios (Matthews et al., 1998); and (2) these variations reflect, in part, Na loss from molten Na-melilite during the experiment.

We evaluated the effects of Na loss by examining relationships between $\Delta^{18}O_{CO2\text{-melt}}$ and both the final Na_2O concen-

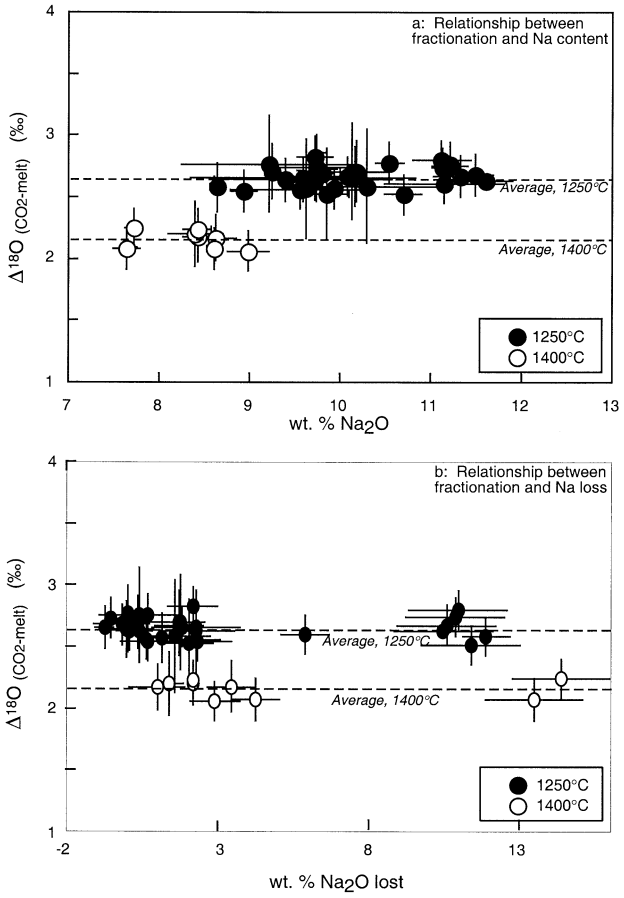

Fig. 3. (a) Comparison of measured fractionations between CO_2 and melt after 24 or more hours at 1250°C (filled circles) or after 7 or more hours at 1400°C (unfilled symbols) with the Na_2O contents of glasses at the end of the experiment. Horizontal dashed lines show the average measured fractionations at the relevant temperatures. Error bars are $\pm 2\sigma$. (b) Comparison of measured fractionations between CO_2 and melt with the difference between initial and final Na_2O contents of glasses (i.e., the amount of Na lost during the experiment). Symbols, error bars and horizontal dashed lines are as in panel a.

trations of quenched glasses and the amount of Na_2O they lost over the course of each experiment (i.e., $Na_2O_{initial}$–Na_2O_{final}). Figure 3 shows the results of this analysis. Values of $\Delta^{18}O_{CO2\text{-}melt}$ are independent of both final Na_2O content (Fig. 3a) and amount of Na_2O lost (Fig. 3b) over wide ranges of both variables and at both 1250 and 1400°C. On this basis, we conclude that, regardless of the mechanism, variation in Na concentration has little or no effect on the final $\Delta^{18}O_{CO2\text{-}melt}$ value compared to the reproducibility of our experiments. This result is consistent with the known relationships between reduced partition function ratios and chemical composition in minerals; i.e., based on the method of Ganor et al. (1994) and according to the small variation in the relative proportions of Si, Al and Ca of the run products (see analytical protocol), variations of Na content between run products is predicted to have ~0.1‰ or less on the CO_2-melt fractionation factor. Moreover, although Na loss from silicate melt by evaporation into a vacuum may transiently affect the $\delta^{18}O$ of the residual melt, isotopic exchange between CO_2 and melt during our experiments is rapid and plausibly overwhelms this effect (Fig. 2).

3.3. Estimation of the Rate of Oxygen Diffusion in Na-Rich Melilite Melt

We can use the rate at which Na-rich melilite melt approaches isotopic equilibrium with coexisting vapor to estimate the oxygen self-diffusion coefficient in that melt if the following two assumptions are made: (1) The isotopic composition of vapor is constant during isotopic exchange; (2) convection inside the melt drop is negligible; and (3) the melt droplet is spherical (note that somewhat more complex shapes are observed for some droplets). Given these assumptions, the oxygen self-diffusion coefficient, D, can be calculated using the following equation (Jost 1960):

$$\frac{\delta_f - \delta_e}{\delta_i - \delta_e} = \frac{6}{\pi^2} \sum_{n=1} \frac{1}{n^2} exp\left[\frac{-n^2\pi^2 D\, t}{r^2}\right], \qquad (1)$$

where r is the radius of the melt drop (in centimeters); t is the duration of the experiment (in seconds); and δ_f, δ_i, and δ_e are the final, initial, and equilibrium $\delta^{18}O_{melt}$ values, respectively. Note that this calculation approximates $^{18}O/^{18}O$ ratios as proportional to $\delta^{18}O$ values; this is not strictly accurate but the error it introduces is insignificant compared to other uncertainties in the calculation. The average radius of melt droplets is ~0.05 cm. Eqn. 1 can be solved for meaningful values of D only if melt undergoes significant isotopic exchange with gas (in practice, changing in $\delta^{18}O$ by several per mil) but does not closely approach isotopic equilibrium with that gas. Eight experiments conducted at 1250°C satisfy this condition, including the four grains of NaMel/1 and four grains of NaMel/2 recovered from experimental run IA/22. Based on these results, Eqn. 1 yields an apparent oxygen self-diffusion coefficient in Na-rich melilite melt of $1.85^{+1.04}_{-0.44} \cdot 10^{-8}$ cm^2/s ($\pm 2\sigma$) at 1250°C. Considering diffusion occurs in melt drops, this value represents the upper bound on the true oxygen self-diffusion coefficient in Na-rich melilitic melt at 1250°C. This value is similar to that previously estimated for basaltic melt at 1280°C and 1 bar (3 to $4 \cdot 10^{-8}$ cm^2/s; Muehlenbachs and Kushiro, 1974). Note that we did not conduct any experiments at 1400°C that would allow determination of the oxygen self-diffusion coefficient, but Canil and Muehlenbachs (1990) measured an oxygen self-diffusion coefficient in basaltic melt of $2 \cdot 10^{-7}$ cm^2/s at 1400°C; this value suggests that ~1 mm diameter melt drops would equilibrate with coexisting vapor within 4 to 5 h, consistent with our experimental result that melt-vapor fractionations are 'bracketed' in 7 to 8 h.

4. DISCUSSION

4.1. Summary of Oxygen Isotope Fractionations Involving Silicate Melts

Our results define the oxygen isotopic fractionation between CO_2 and Na-melilitic melt to be 2.65±0.25 ‰ (2σ, n=92; standard error of the mean = 0.03 ‰, 2σ) at 1250°C and 2.16±0.16 ‰ (2σ, n=17; standard error of the mean = 0.04 ‰, 2σ) at 1400°C. In this section we compare these data to previous studies of oxygen isotope fractionations involving

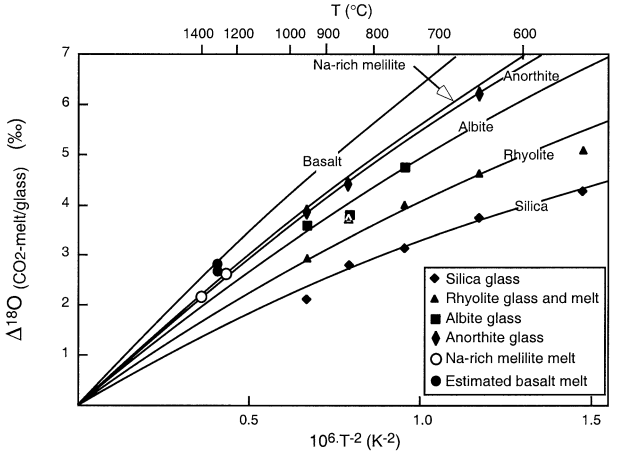

Fig. 4. Plot vs. $10^6\ T^{-2}$, where T is the experimental temperature in K, of measured oxygen isotopic fractionations between CO_2 and Na-rich melilite melt (this study; open circles), anorthite glass (filled long diamonds; data of Matthews et al., 1998), albite glass (filled squares; data of Matthews et al., 1994), rhyolite glass and melt (filled triangles; data of Palin et al., 1996), and silica glass (filled equant diamonds; data of Stolper and Epstein, 1991), and an estimate of the CO_2-basalt melt fractionation (filled circles; based on data from Muehlenbachs and Kushiro, 1974). Error bars are omitted for clarity; see text, tables and references listed above for error estimates. Curves are fitted polynomials used as the basis for estimating the temperature dependence of reduced partition function ratios of melts and glasses; see text and Table 4 for details.

silicate melts and glasses and derive expressions for the reduced partition function ratios of silicate melts examined in this study and these previous studies.

Figure 4 summarizes results of this study (open circles) and those of previous experimental studies of oxygen isotopic fractionations between CO_2 and silicate melts and glasses (filled symbols). All measured fractionations are plotted vs. T^{-2}. Our results cannot be directly compared to the experiments of Muehlenbachs and Kushiro (1974) on basaltic melt because those experiments report isotopic compositions of basalt glass, plagioclase, and enstatite that had been exposed to the same stream of CO_2 or O_2 gas, but not the isotopic composition of the gas itself. Nevertheless, we can estimate the CO_2-basalt fractionation consistent with their results by combining them with independent estimates of the reduced partition function ratios of plagioclase or enstatite and CO_2. Plagioclase is more fully described by experimental and theoretical studies of oxygen isotope fractionations than is enstatite, and therefore for this purpose we focus on Muehlenbachs and Kushiro's report that basalt-plagioclase (An_{80}-An_{100}) fractionations at 1300°C are approximately −0.35 ‰ (visually estimated from the diagram presented in Muehlenbachs and Kushiro, 1974). Combining this result with reduced partition function ratios for CO_2 and An_{90}-plagioclase from Chacko et al. (1991) and Clayton and Kieffer (1991), yields a value for $\Delta^{18}O_{CO2\text{-}basalt}$ of 2.8 ‰ ($2\sigma \approx 0.4$‰) at 1300°C. This indirect estimate of the CO_2-basalt melt fractionation is shown as a filled circle in Figure 4. Note that our results on Na-melilitic melt and the estimates for basaltic melt overlap within error, verifying the premise of this investigation that Na-melilitic melt is a reasonable Fe-free analog for basaltic melts.

Also plotted in Figure 4 are fits to each data set of curves of the form

$$\Delta^{18}O_{CO2\text{-}melt} = A \cdot x + B \cdot x^2 + C \cdot x^3, \quad (2)$$

where $x = 10^6 \cdot T^{-2}$. This equation has the advantage that temperature dependence of reduced partition function ratios [$1000 \cdot \ln(Q'/Q)$] is well described by third-order polynomial functions of T^{-2} (e.g., Clayton and Kieffer, 1991), and differences in $\delta^{18}O$ between coexisting phases can be stated in terms of their reduced partition function ratios through the relationship:

$$\Delta^{18}O_{a-b} = 1000 \cdot \ln(Q'/Q)_a - 1000 \cdot \ln(Q'/Q)_b, \quad (3)$$

In particular, the reduced partition function ratio for CO_2 are well known and can be fit precisely as a third-order polynomial function of T^{-2} (Chacko et al., 1991). Therefore, by using this functional form, we can deduce equations describing reduced partition function ratios for silicate melts as functions of temperature that are consistent with previous treatments.

We fit curves having the form of Eqn. 2 to the data shown in Figure 4 by 'scaling' theoretically calculated curves for CO_2-mineral fractionations. For each melt or glass shown in Figure 4, we scaled (i.e., multiplied all three coefficients in Eqn. 2 by a constant) the theoretically determined reduced partition function ratio of a known mineral, and combined it with the CO_2 reduced partition function ratio (a third-order fit based on data from Chacko et al., 1991) to model the temperature dependence of CO_2-melt/glass fractionation. For each melt composition, the scaling factor was adjusted to minimize the misfit between the curve and measured values of $\Delta^{18}O_{CO2\text{-}melt}$. The quartz reduced partition function ratio was scaled to fit the CO_2-silica glass data; the albite ratio was scaled to fit the CO_2-albite melt and CO_2-rhyolite data; the anorthite ratio was scaled to fit our CO_2-Na-rich melilitic melt data and the CO_2-anorthite glass data; and the diopside ratio was scaled to fit the estimated CO_2-basalt fractionation. The resulting fitted curves are plotted in Figure 4 as solid curves for direct experimental constraints and as a dashed curve for the inferred CO_2-basalt fractionation. Equations for the reduced partition function ratios used to calculate the curves shown in Figure 4 are given in Table 4.

The equations in Table 4 describing reduced partition function ratios of silicate melts and glasses can be compared with reduced partition function ratios of other oxygen-bearing compounds to estimate isotopic fractionations involved in partial melting of mantle and crustal rocks and crystallization and degassing of magmas. A full exploration of such uses of these data is beyond the scope of this paper; however, we present in Figure 5a summary of some of the most important fractionations involving silicic (Fig. 5a) and mafic (Fig. 5b) magmas. These figures are based on the expressions for reduced partition function ratios for melts given in Table 4 and similar equations for reduced partition function ratios of minerals from Clayton and Kieffer (1991).

Several generalizations can be deduced from Figure 4 and 5: (1) Oxygen isotope fractionations among silicate minerals and melts for temperatures and melt compositions typical of siliceous magmas span a range of ~2 to 3 per mil, with higher $\delta^{18}O$ values in minerals and melts with high ratios of network-forming cations (Si and Al) to network-modifying cations (Na,

Table 4. Coefficients of reduced partition function ratio

Material	A*	B*	C*	Reference#	Fit parameters&
Silica glass	12.516	−0.382	0.0127	1	Quartz · 1.033
Rhyolite melt and glass	11.691	−0.342	0.0109	2	Albite · 1.050
Albite glass	10.822	−0.317	0.0101	3	Albite · 0.972
Anorthite glass	10.223	−0.277	0.0084	4	Anorthite · 1.023
Na-melilite melt	10.053	−0.273	0.0082	this study	Anorthite · 1.006
Basalt melt	9.191	−0.198	0.0053	5	Diopside · 0.995
Quartz	12.116	−0.370	0.0123	6	n.a.
Albite	11.134	−0.326	0.0104	6	n.a.
Anorthite	9.993	−0.271	0.0082	6	n.a.
Diopside	9.237	−0.199	0.0053	6	n.a.
Forsterite	8.326	−0.142	0.0032	6	n.a.
CO_2	16.518	−1.191	0.0648	7	n.a.

* 1000 ln (Q′/Q) = $A \cdot x + B \cdot x^2 + C \cdot x^3$, where $x = 10^6 \cdot T^{-2}$

1: Stolper and Epstein, 1991; 2: Palin et al., 1996; 3: Matthews et al., 1994; 4: Matthews et al., 1998; 5: Muehlenbachs and Kushiro, 1974; 6: Clayton and Kieffer, 1991; 7: Chacko et al., 1991

& A, B and C terms fit by multiplying those for the listed mineral by the listed coefficient.

Ca, and Mg; Fig. 5a). (2) Fractionations at the higher temperatures and more basic mineral and melt chemistries typical of mafic magmas are smaller overall (≤1 per mil total range), but they follow a pattern similar to that for felsic compositions in that Si- and Al-rich minerals and melts are higher in $\delta^{18}O$ than those that are Si- and Al-poor (Fig. 5b). (3) Melts and glasses have oxygen isotope partitioning behaviors broadly similar to those of chemically identical feldspars minerals (e.g., Matthews et al., 1994, 1998), but this correspondence is not perfect: silica glass differs from quartz (Stolper and Epstein, 1991). Diopside appears to be the mineral that is most similar in its oxygen isotope fractionation to basalt and Na-melilite is most similar to anorthite. (4) The curves in Figure 5b predict that at magmatic temperatures $\Delta^{18}O_{basalt\text{-}olivine}$ approximately equals 0.4‰ and $\Delta^{18}O_{basalt\text{-}plagioclase}$ approximately equals −0.3‰. These values agree well with fractionations between glasses and coexisting phenocrysts reported on several terrestrial basalts (Eiler et al., 1995; 2000). Eiler et al. (2000) measured, for oceanic-arc lavas, an average glass-olivine fractionation of 0.36±0.22‰ (2σ) and an average plagioclase-olivine fractionation of 0.65±0.14‰ (2σ). These ranges enclose most of groundmass-phenocryst fractionations previously obtained by conventional fluorination on terrestrial and lunar basalts (e.g., Clayton et al., 1971; Anderson et al., 1971; Kyser et al., 1982). However, larger basalt-olivine fractionations have been reported by some other studies (e.g., Kyser et al., 1981; Macpherson and Mattey, 1998; Macpherson et al., 1998) and are similar to our estimate for $\Delta^{18}O_{Namelilite\text{-}olivine}$ that approximately equals 0.7‰ at 1300°C.

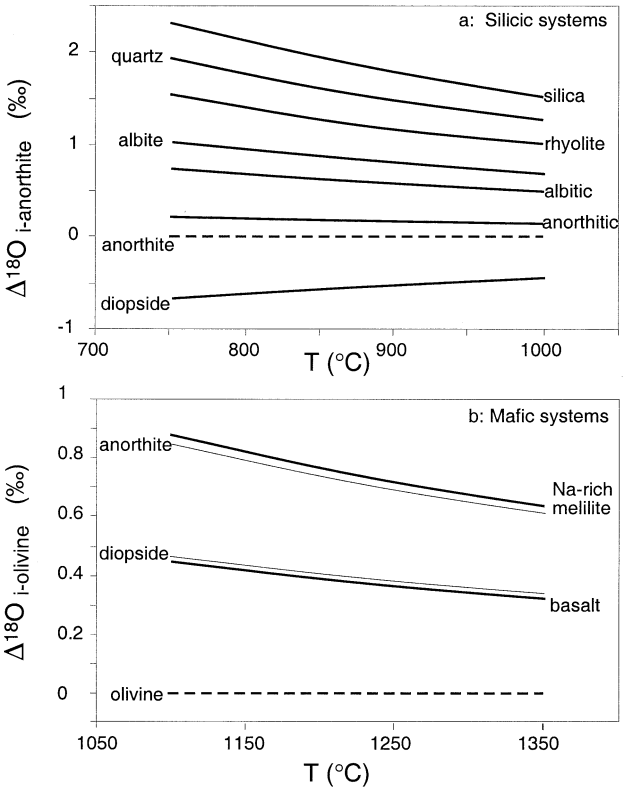

Fig. 5. Predicted fractionations among select minerals and melts for temperatures and compositions relevant to silicic magmatic systems (panel a) and basaltic magmatic systems (panel b). All fractionations are based on equations describing reduced partition function ratios presented in Table 4.

4.2. Methods of Interpolation and Extrapolation to Other Silicate Melt Compositions

The oxygen isotope partitioning behaviors of natural silicate melts are more difficult to describe fully by experiment than those of minerals because melts vary continuously and independently in the concentrations of many components whereas minerals follow stoichiometric solid solutions in which crystallographic constraints restrict the number of end members that need to be studied. Therefore, it would be useful to extract from experiments simple relationships that will allow interpolation and extrapolation to experimentally unexplored melt compositions. Relationships among reduced partition function ratios of melts and glasses (Table 4; Figs. 4 and 5) suggest that one basis for interpolation might be differences in proportions of network-forming cations, which appear systematically to

concentrate ^{18}O relative to ^{16}O (e.g.,; Taylor and Epstein, 1962; Garlick, 1966). Alternatively, one could call on the approximation, known to be valid for some mineral solid solutions, that reduced partition function ratios of mixtures can calculated as weighted sums of the reduced partition function ratios of their end members (O'Neil and Taylor, 1967; Palin et al., 1996). The following sections explore these two alternatives in more detail.

4.2.1. The Garlick index

Garlick (1966) observed that oxygen isotope fractionations among minerals in igneous and metamorphic rocks follow a pattern that, at any given temperature, phases rich in Si and Al concentrate ^{18}O relative to coexisting Si- and Al-poor minerals. He described this pattern using a formalism that is now commonly called the Garlick index, I, defined as follows:

$$I = (C_{Si} + 0.58.C_{Al})/\sum C_i \text{ for all cations, } I' \qquad (4)$$

where the concentration (C_i) of a given cation in a mineral is calculated as the molar concentration of its oxide (e.g., SiO_2, $AlO_{1.5}$, CaO, etc) multiplied by the number of oxygen atoms associated with that cation in the mineral formula (i.e., $\times 2$ for Si; $\times 1.5$ for Al; $\times 1$ for Ca, Mg or Fe^{+2}); concentrations are equivalent to mole fraction where each component is defined on a single-oxygen basis. This index can be used to model oxygen isotope fractionations between two minerals through the following relationship (Ganor et al., 1994):

$$\Delta^{18}O_{i-j} = k \cdot (I_i - I_j) \cdot 10^6/T^2, \qquad (5)$$

where i and j are two different silicate minerals and k is a constant derived by fitting Eqn. 5 to experimental data or measurements from natural rocks equilibrated at known temperatures. Several values of k have been proposed; most recently, Ganor et al. (1994) gave a value of $k = 6.8 \pm 1$ (2σ) based on data on experimental and natural pairs of anhydrous silicates, primarily at temperatures of 500 to 1000°C. Matthews et al. (1998) proposed that oxygen isotope fractionations involving silicate melts can be estimated by calculating the Garlick index of the melt and using Eqn. 5 with the value of k derived by Ganor et al. (1994). This approach is straightforward and agrees approximately with measured fractionations between coexisting phenocrysts and volcanic glasses (Matthews et al., 1998).

Figure 6 compares the Garlick index (Eqn. 4) to the reduced partition function ratios for the six melt compositions that have been investigated experimentally. The Garlick index is linearly correlated with the reduced partition function ratio at any given temperature and thus is a reasonable means of interpolating among known silicate melts using at any assumed temperature. All data in Figure 6 can be described with the equation: $1000 \cdot \ln(Q'/Q) = (k \cdot I + C)\ 10^6/T^2$; where k equals 8.6 ± 2.0 (2σ) and C equals 3.6 (2σ = 0.7 at 1300°C). This method of interpolation has the advantages of being easily integrated with data describing reduced partition function ratios of any other phase (silicate or otherwise) and of being directly based on experimental data for silicate melts and glasses. Combining the equation above for melts with the estimated reduced partition function ratios from Clayton and Kieffer (1991) for olivine (see Table 4), we calculate a value for $\Delta^{18O}_{MORB\text{-}olivine}$ of 0.55‰ (2σ, 0.33‰) at 1300°C. This value is similar to that calculated by Matthews et al. (1998). Note that until more experiments are available, this approach must be applied cautiously to modeling fractionation factors involving melts with high concentrations of cations that are not well represented by melts and glasses examined by previous experiments (e.g., Ti).

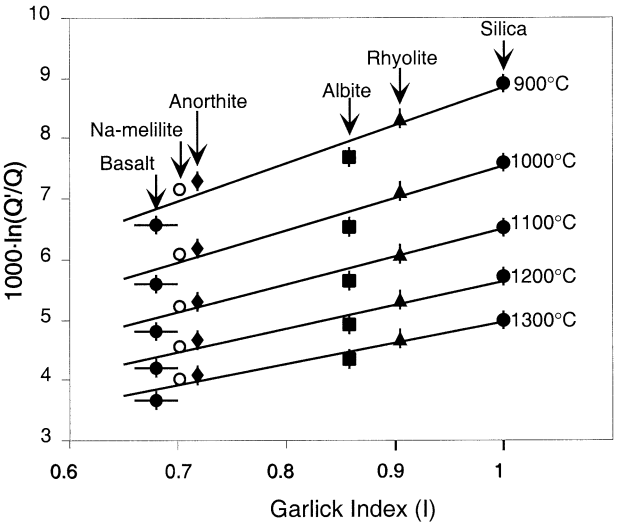

Fig. 6. Comparison of reduced partition function ratio with the 'Garlick' index (I) for silicate melts considered in this paper and at several representative temperatures. All reduced partition function ratios are calculated using equations given in Table 4. The horizontal bars through points for basalt melt indicate the typical range in Garlick index of basaltic rock. According to Clayton and Kieffer (1991), uncertainties on reduced partition function ratios are assumed to be comparable in magnitude to the errors on the experimental data. Errors bars on chart represent 1σ, deduced from experimental studies (i.e., Stolper and Epstein, 1991; Matthews et al., 1994; Palin et al., 1996 Matthews, unpublished report; and this study).

4.2.2. Normative abundance model

Palin et al. (1996) showed that the oxygen isotope fractionation between CO_2 and rhyolite glass at a given temperature can be approximated by the weighted sum of the CO_2-silica glass and CO_2-albite glass at that temperature, where the proportions of each are taken to be the normative abundances of silica and alkali feldspar in rhyolite (where mole fractions of each component are calculated on a single oxygen basis). Eiler (2001) extended this approach by suggesting that oxygen isotope fractionations involving silicate melts other than rhyolite can be approximated by calculating reduced partition function ratios of melts as the weighted sum of their normative mineral constituents (again, on a single oxygen basis) or, when known, the molten equivalents of those constituents. The advantages of this approach are that it draws upon the large data base of experimental studies of oxygen isotope fractionations involving minerals, it involves a straightforward normative calculation, and it provides a basis for predicting fractionations involving melts with unusual chemical compositions. The principal disadvantage is that there are few data on compositionally complex silicate melts that explicitly test this model. It successfully describes rhyolite glass as a mixture of albite glass and silica

glass (Palin et al., 1996). The normative constituents of Na-melilite have less well known oxygen isotope partitioning behavior, but combining experimental fractionation data on calcite-gehlenite (see review Chacko et al., 2001) with an estimate of sodamelilite-gehlemite fractionation based on the protocol of Kohn and Valley (1998), yields to a reduced partition function ratio for crystalline Na-melilite within 0.1 per mil that determined by our experiments. Although the chemical composition of the basalt studied by Muehlenbachs and Kushiro (1974) was not reported, Eiler (2001) showed that the normative model predicts that typical basaltic compositions have reduced partition function ratios within ~0.2 to 0.3 per mil of that we estimate here based on the experiments of Muhlenbachs and Kushiro (1974). Thus, although there are not many experimental determinations of fractionation factors involving melts, the normative model provides a useful first step for estimating their oxygen isotope fractionations, and with further calibration, may provide a precise approach to their calculation.

5. SUMMARY

We determined the oxygen isotope fractionation between CO_2 and Na-rich melilite melt at ~1 bar pressure and 1250 and 1400°C. The fractionation factor constrained by bracketed experiments, $1000 \cdot \ln\alpha_{CO2\text{-}Na\ melilite}$, is 2.65±0.25 ‰; 2σ'3b ± 0.03 ‰, 2σ standard error at 1250°C and 2.16±0.16 ‰; 2σ'3b ± 0.04 ‰, 2σ standard error at 1400°C. Abundances of Na_2O in quenched glasses and amounts of Na lost from melt over the course of each experiment have no measurable influence on the fractionation factor. The kinetics of CO_2-melt exchange at 1250°C are consistent with an oxygen self diffusion coefficient of $\sim 2 \cdot 10^{-8}$ cm^2/s—similar to that previously determined for basalt melt (Muehlenbachs and Kushiro, 1974). The time-scale for CO_2-melt exchange at 1400°C are consistent with measured rates of oxygen self diffusion in basalt melt.

Combination of our results with estimates of the reduced partition function ratio for CO_2 (Chacko et al., 1991) results in a polynomial expression for the reduced partition function ratio for Na-rich melilite melt as a function of temperature. Similar calculations using previously reported or inferred CO_2-melt and CO_2-glass fractionations give expressions for the reduced partition function ratios of silica, rhyolitic, feldspathic and basaltic melts and glasses as functions of temperature. Measured oxygen isotope fractionation between CO_2 and Na-melilitic melt and the inferred fractionation between CO_2 and basaltic melt are similar, confirming the utility of Na-melilite as an Fe-free analog for basaltic liquids.

We suggest two methods for generalizing available data to estimate fractionation of oxygen isotopes between CO_2 and silicate melt compositions that have not yet been examined experimentally: (1) Interpolation among experimentally known melt compositions using the 'Garlick index', a measure of the molar fraction of oxygen in the melt that is in tetrahedral coordination. Although more data are needed to establish the limits of this approach, known reduced partition function ratios of melts and glasses are linearly correlated with the Garlick index at any given temperature. (2) Approximation of the reduced partition function ratios of unknown and compositionally complex melts as the weighted sums of mineral end members corresponding to their normative constituents. Although data are currently available on only a limited number of melt compositions, available data suggest that both of these methods are accurate to within ca. 0.3 to 0.4 per mil at magmatic temperatures. Additional data are needed to test the validity of these approximations to the range of common magmatic liquids.

Acknowledgments—We thank John Beckett for invaluable assistance on experimental procedures, Nami Kitchen for help in the stable isotope laboratory, and Reid Cooper and his colleagues at Corning for their help preparing NaMel/1 glass. We thank Juske Horita and anonymous reviewers for help in improving our manuscript. This work was supported by BSF Grant BSF 97–00454, DOE grant DE-FG03–85ER13445, and NSF grants EAR-0095897 and OCE-0095897.

Associate editor: J. Horita

REFERENCES

Anderson A. T., Clayton R. N., and Mayeda T. K. (1971) Oxygen isotope thermometry of mafic igneous rocks. *J. Geol.* **79,** 715–729.

Armstrong J. T (1995) CITZAF: a package of correction programs for the quantitative electron microbeam X-ray analysis of tickpolished materials, thin films, and particles. *Microbeam Anal.* **4,** 177–200.

Baertschi P. (1976) Absolute ^{18}O content of standard mean ocean water. *Earth Planet. Sci. Lett.* **31,** 341–344.

Bottinga Y. and Javoy M. (1975) Oxygen isotope partitioning among the minerals in igneous and metamorphic rocks. *Rev. Geophys. Space Phys.* **13,** 401–418.

Canil D. and Muehlenbachs K. (1990) Oxygen diffusion in an Fe-rich basalt melt. *Geochim. Cosmochim. Acta* **54,** 2947–2951.

Chacko T., Mayeda T. K., Clayton R. N., and Goldsmith J. R. (1991) Oxygen and carbon isotope fractionations between CO_2 and calcite. *Geochim. Cosmochim. Acta* **55,** 2867–2882.

Chacko T., Cole D. R. and Horita J. (2001) Equilibrium oxygen, hydrogen and carbon isotope fractionation factors applicable to geologic systems. In *Stable Isotope Geochemistry* (eds. J. W. Valley and D. Cole) *Rev. Mineral. Geochem.* **43,** Chap. 1, pp.1–81. Mineral. Soc. Am.

Chiba I., Chacko T., Clayton R. N., and Goldsmith J. R. (1989) Oxygen isotope fractionations involving diopside, forsterite, magnetite and calcite: application to geothermometry. *Geochim. Cosmochim. Acta* **53,** 2985–2995.

Clayton R. N. and Kieffer S. W. (1991) Oxygen isotopic thermometer calibrations. In *Stable Isotope Geochemistry: A Tribute to Samuel Epstein, The Geochemical Society Special Publication, Special Publication, No. 3.* (ed. H. P. Taylor Jr. et al.) *Geochem. Soc. Spec. Pub.* **3,** pp. 3–10. The Geochemical Society.

Clayton R. N., Onuma N., and Mayeda T. K. (1971) Oxygen isotope fractionations in Apollo 12 rocks and soils. *Geochim. Cosmochim. Acta* **2,** 1417–1420.

Clayton R. N., Goldsmith J. R. and Mayeda T. K. (1989) Oxygen isotope fractionations in quartz, albite, anorthite and calcite. *Geochim. Cosmochim. Acta* **53,** 725–733.

Corrigan G. and Gibb F. G. (1979) The loss of Fe and Na from a basaltic melt during experiments using the wire-loop method. *Mineral. Mag.* **43,** 121–126.

Darken L. S. and Gurry R. W. (1945) The system iron-oxygen. I. The wüstite field and related equilibria. *J. Am. Chem. Soc.* **67,** 1398–1412.

Davidson J. P. and Harmon R. S. (1989) Oxygen isotope constraints on the petrogenesis of volcanic arc magmas from Martinique, Lesser Antilles. *Earth Planet. Sci. Lett.* **95,** 255–270.

Deines P. (1977) On the oxygen isotope distribution among mineral triplets in igneous rocks. *Geochim. Cosmochim. Acta* **41,** 1709–1730.

Donaldson C. H. (1979) Composition changes in a basalt melt contained in a wire loop of $Pt_{80}Rh_{20}$: effects of temperature, time, and oxygen fugacity. *Mineral. Mag.* **43,** 115–119.

Donaldson C. H., Williams R. J., and Lofgren G. (1975) A sample holding technique for study of crystal growth in silicate melts. *Am. Mineral.* **60,** 324–326.

Eiler J. M. (2001) Oxygen isotope variations of basaltic lavas and upper mantle rocks. In *Stable Isotope Geochemistry* (eds. J. W. Valley and D. Cole) *Rev. Mineral. Geochem.* **43,** Chap. 5, pp. 319–364. Mineral. Soc. Am.

Eiler J. M., Farley K. A., Valley J. W., Stolper E. M., Hauri E. and Craig H. (1995) Oxygen isotope evidence against bulk recycled sediment in the source of Pitcairn Island lavas. *Nature* **377,** 138–141.

Eiler J. M., Crawford A., Elliott T., Farley K. A., Valley J. W. and Stolper E. M. (2000) Oxygen isotope geochemistry of oceanic-arc lavas. *J. Petrol.* **41,** 229–256.

Ganor J., Matthews A. and Schliestedt M. (1994) Post-metamorphic low $\delta^{13}C$ calcite in the Cycladic complex (Greece) and their implications for modeling fluid infiltration processes using carbon isotope composition. *Eur. J. Mineral.* **6,** 365–379.

Garlick G. D. (1966) Oxygen isotope fractionation in igneous rocks. *Earth Planet. Sci. Lett.* **1,** 361–368.

Huebner J. S. (1975) Oxygen fugacity values of furnace gas mixture. *Am. Mineral.* **60,** 815–823.

Jost (1960) Diffusion in solids, liquids, gases. New York. Academic Press, N.Y., 558 pp.

Kalamarides R. I. (1986) High-temperature oxygen isotope fractionation among the phases of the Kiglapait intrusion, Labrador, Canada. *Chem. Geol. (Isot. Geosci. Sect).* **58,** 303–310.

Kohn S. C., Brooker R. A. and Dupree R. (1991) ^{13}C MAS NMR: A method for studying CO_2 speciation in glasses. *Geochim. Cosmochim. Acta* **55,** 3879–3884.

Kohn M. J. and Valley J. W. (1998) Oxygen isotope geochemistry of amphiboles: Isotopic effects of cation substitutions in minerals. *Geochim. Cosmochim. Acta* **62,** 1947–1958.

Kyser T. K., O'Neil J. R. and Carmichael I. S. E. (1981) Oxygen isotope thermometry of basic lavas and mantle nodules. *Contrib. Mineral. Petrol.* **77,** 11–23.

Kyser T. K., O'Neil J. R. and Carmichael I. S. E. (1982) Genetic relations among basic lavas and ultramafic nodules: evidence from oxygen isotope compositions. *Contrib. Mineral. Petrol.* **81,** 88–102.

Macpherson C. G. and Mattey D. P. (1998) Oxygen isotope variations in Lau Basin lavas. *Chem. Geol. (Isot. Geosci. Sect).* **144,** 177–194.

Macpherson C. G., Gamble J. A. and Mattey D. P. (1998) Oxygen isotope geochemistry of lavas from an oceanic to continental arc transition, Kermadec-Hikurangi margin, SW Pacific. *Earth Planet. Sci. Lett.* **160,** 609–621.

Matsuhisa Y., Goldsmith J. R. and Clayton R. N. (1979) Oxygen isotopic fractionation in the system quartz-albite-anorthite-water. *Geochim. Cosmochim. Acta* **43,** 1131–1140.

Matthews A., Goldsmith J. R. and Clayton R. N. (1983) Oxygen isotope fractionations involving pyroxenes: The calibration of mineral pair geothermometers. *Geochim. Cosmochim. Acta* **47,** 631–344.

Matthews A., Palin J. M., Epstein S. and Stolper E. M. (1994) Experimental study of $^{18}O/^{16}O$ partitioning between crystalline albite, albitic glass and CO_2 gas. *Geochim. Cosmochim. Acta* **58,** 5255–5266.

Matthews A., Stolper E. M., Eiler J. M., and Epstein S. (1998) Oxygen isotope fractionation among melts, minerals and rocks (abst.). *VIII Goldschmidt Conference; Toulouse (France); Mineral. Mag.* **62A,** 971–972.

Muehlenbachs K. and Kushiro I. (1974) Oxygen isotope exchange and equilibrium of silicates with CO_2 and O_2. *Carnegie Inst. Wash. Yearb.* **73,** 232–236.

Mysen B. O. and Virgo D. (1980) Solubility mechanisms of water in basalt melt at high pressures and temperatures: $NaCaAlSi_2O_7$-H_2O as a model. *Am. Mineral.* **65,** 1176–1184.

O'Neil J. R. (1986) Theoritical and experimental aspects of isotopic fractionation. In *Stable Isotopes in High Temperature Geological Processes* (eds. J. W. Valley, H. P. Taylor and J. R. O'Neil) *Rev. Mineral.* **16,** Chap. 1, pp. 1–40. Mineral. Soc. Am.

O'Neil J. R. and Taylor H. P. (1967) The oxygen isotope and cation exchange chemistry of feldspars. *J. Chem. Phys.* **51,** 5547–5558.

Palin J. M., Epstein S. and Stolper E. (1996) Oxygen isotope partitioning between rhyolitic glass/melt and CO_2: An experimental study at 550–950°C and 1 bar. *Geochim. Cosmochim. Acta* **60,** 1963–1973.

Stolper E. and Epstein S. (1991) An experimental study of oxygen isotope partitioning between silica glass and CO_2 vapor. In *Stable Isotope Geochemistry: A Tribute to Samuel Epstein, The Geochemical Society Special Publication, Special Publication, No. 3.* (ed. H.P. Taylor Jr. et al.) *Geochem. Soc. Spec. Pub.* **3**, 35–51. The Geochemical Society.

Taylor H. P. and Epstein S. (1962) Relationship between O^{18}/O^{16} ratios in coexisting minerals of igneous and metamorphic rocks. Part I: Principles and experimental results. *Bull. Geol. Soc. Am.* **73,** 461–480.

Taylor H.P. and Sheppard S.M. F (1986) Igneous rocks:I. Processes of isotopic fractionation and isotope systematics. In *Stable Isotopes in High Temperature Geological Processes* (eds. J. W. Valley, H. P. Taylor and J. R. O'Neil) *Rev. Mineral.* **16,** Chap. 8, pp. 227–272. Mineral. Soc. Am.

Tsuchiyama A., Nagahara H. and Kushiro I. (1981) Volatilization of sodium from silicate melt spheres and its application to the formation of chondrules. *Geochim. Cosmochim. Acta* **45,** 1357–1367.

Valley J. W., Kitchen N., Kohn M. J., Niendorff C. R. and Spicuzza M. J. (1995) Strategies for high precision oxygen isotope analysis by laser fluorination. *Geochim. Cosmochim. Acta* **59,** 5223–5231.